Astronomy & Astrophysics manuscript no. output
May 7, 2026

Low-energy electron-driven functionalization of benzene–water ices to phenol

H. Abdoul-Carime[1]⋆, E. Ogden[2], L. Biennier[2], S. Carles[2], and F. Rabilloud[3]

[1] Université Claude Bernard Lyon 1, Institut de Physique des 2 Infinis, CNRS/IN2P3, UMR5822, F-69622 Villeurbanne, France
[2] Institut de Physique de Rennes, UMR CNRS 6251, Université de Rennes, Campus de Beaulieu, 35042 Rennes Cedex, France
[3] Université Claude Bernard Lyon 1, CNRS, Institut Lumière Matière, UMR 5306, F-69100 Villeurbanne, France 32

May 7, 2026

ABSTRACT

Low-energy electrons abundantly generated by galactic cosmic radiation are expected to play a central role in the radiation chemistry of interstellar and cometary ices, yet their capacity to drive specific bond-forming reactions in simple aromatic systems remains poorly constrained. Here, sub-12 eV electrons were used to irradiate mixed benzene (C_6H_6)–water ices under cryogenic conditions, which led to the selective formation of phenol (C_6H_5OH) via C–O bond formation at the aromatic ring. Energy-resolved measurements show that the phenol yield is governed by resonant processes, consistently with dissociative electron attachment and electronically excited states of the condensed benzene–water matrix. Temperature-programmed desorption combined with mass-spectrometry diagnostics allowed the direct quantification of phenol production. These results demonstrate that low-energy electrons alone can promote net hydroxylation of benzene in icy environments, providing a previously underappreciated route to phenolic species in dense clouds, star-forming regions and irradiated icy bodies, and highlighting electron-induced functionalization as a key driver of aromatic complexity in astrochemical ices.

Key words. benzene - water - ices - phenol synthesis - low-energy electrons - TDDFT calculations

1. Introduction

Aromatics permeate every corner of our Universe (Kaiser & Hansen 2021). For decades, the presence of polycyclic aromatic hydrocarbons (PAHs), representing 10–20% of the interstellar carbon, was inferred indirectly (Hrodmarsson et al. 2025); they collectively caused the widespread aromatic infrared bands (AIBs), which dominate the emission spectra of rich-dust astrophysical environments (Leger & Puget 1984; Allamandola et al. 1989). Infrared observations suggested PAHs pervade the interstellar medium (ISM)—as they are particularly abundant in environments associated with star formation—such as photodissociation regions (PDRs), planetary nebulae, and protoplanetary disks. This ubiquity is supported by their detection in primitive extraterrestrial matter, including samples from the Ryugu asteroid (Hayabusa2 probe) (Sabbah et al. 2024) and primitive carbonaceous chondrites such as Murchison (Sephton 2005). Smaller PAH family members have also been detected in comets, such as 81P/Wild 2 (Sandford et al. 2006) and 67P/Churyumov–Gerasimenko (Hänni et al. 2022).

A major breakthrough was the recent radio-detection of specific PAHs—many being derivatives—in the cold, dense Taurus molecular cloud (TMC-1) (see, e.g., Cernicharo et al. 2021; Burkhardt et al. 2021; Cabezas et al. 2025; Wenzel et al. 2024). These discoveries confirm that complex aromatic synthesis is active even in the earliest stages of star and planet formation. Benzene (C_6H_6), the principal building block of PAHs (Langer et al. 2023; Lemmens et al. 2022; Bohm 1992), has been detected in the circumstellar envelopes of the protoplanetary nebulae CRL 618 (Cernicharo et al. 2001) and V353 Aur (Bernard-Salas et al. 2006), but also in meteorites (Meinshein 1963), comets (Schuhmann et al. 2019), and Titan's atmosphere (Coustenis et al. 2007; Yoon et al. 2014). In addition, the presence of benzene has been reported on giant planets (**?**). While not directly observed in cold interstellar clouds due to its lack of a dipole moment, photochemical models predict its abundance there.

Water-rich ices are key constituents of molecular dense clouds and are prevalent throughout the Solar System. These ices serve as reservoirs where a large fraction of aromatic species, including benzene, are expected to freeze onto dust grains due to their low volatility. In a recent study, it was shown that the radiolytic destruction-rate constant of benzene in benzene water ice surpasses that of pure benzene ice (Tribett et al. 2026). The chemical evolution within these cosmic ices—which ultimately populates the gas phase upon sublimation in warmer regions—is fundamentally driven by external energy sources such as high-energy photons, cosmic-ray bombardment, and thermal changes. The interaction of radiation, for example (V)UV-, X-, and cosmic rays, with dense gas or ices produces excited species, ions, radicals, and electrons along the penetration tracks as the first initiating step of complex chemistry (Pimblott & LaVerne 2007; Blanco et al. 2013; McMahon & Prise 2019). While such ion/radical reactions have been studied relatively extensively (see, e.g., Snow & Bierbaum 2008; Arumainayagam et al. 2019; Öberg 2016), and the effect of UV radiation (often generated by cosmic rays exciting H_2 in a process called cosmic-ray-induced photochemistry) is accounted for, the primary synthesis pathway in cold ices may be dominated by a different process. In dense cloud environments, the rate of UV production from the

⋆ Corresponding author: hassan.abdoul-carime@univ-lyon1.fr

Article published by EDP Sciences, to be cited as https://doi.org/10.1051/0004-6361/202659133

Lyman–Werner band of excited H_2 is often considered too low to efficiently drive reactions (Prasad & Tarafdar 1983). In contrast, Galactic cosmic rays generate a massive flux of ballistic secondary electrons as they pass through the ice [1].

The role of ballistic secondary electrons in astrochemistry has only been demonstrated in the last decades (Pan et al. 2004; Boyer et al. 2016; Abdoul-Carime et al. 2022). Electron-induced processes represent a new frontier in the synthesis of complex molecules in interstellar ices (Mason et al. 2014; Arumainayagam et al. 2019). These particles are generated with an energy distribution below 15 eV (Pimblott & LaVerne 2007; Mucke et al. 2010) and are capable of initiating molecular fragmentation and rearrangement of chemical bonds through the formation of subproducts (Abdoul-Carime et al. 2024b), in the same manner as photons of the similar energy range (McMahon & Prise 2019; Bulak et al. 2013), however via different processes and efficiencies (in terms of fragmentation cross-sections). For instance, it has been shown that irradiation of acetonitrile-water films by low-energy electrons (LEEs; $\sim 10^{14}$ e/cm^2) (Abdoul-Carime et al. 2022) and by high-density UV photons (i.e., $\sim 10^{16}$ photons/cm^2) (Bulak et al. 2013) results in the synthesis of both methanol and glycolonitrile species, which is indicative of the effectiveness of electrons to initiate processes. It is noteworthy that low-energy (4–20 eV) electron irradiation of ammonia:acetic acid ices synthesizes glycine amino acid via radical–radical reactions that arose in the vicinity of the condensed reactants (Lafosse et al. 2006). Unlike energetic (>20 eV) particles, LEEs can selectively dissociate individual specific molecules, as has been shown in benzonitrile:water films (Abdoul-Carime et al. 2024b). Indeed, irradiation by 3 eV electrons can only trigger reactivity by fragmenting aromatic compounds that compose the film alone. This leaves water molecules unaffected by dissociation, which only arises at energies above 6 eV.

To study the crucial synthesis of functionalized aromatics in the ice phase, we focused on phenol (C_6H_5OH), the simplest oxygenated aromatic molecule. In this work, we investigated the chemistry of benzene:water films irradiated by low-energy electrons (LEEs < 12 eV). While proton, UV photon (Ruiterkamp et al. 1990), and γ-beam (Kodera & Hikida 1990) irradiation of such films has been explored previously, the production of phenol was not reported. Here, we examine the effects of electron irradiation at different energies employing a combined experimental and theoretical approach. Our goal is to elucidate the fragmentation of benzene and water induced by LEEs and the subsequent reactions leading to the formation of new, more complex species, such as phenol.

2. Methods

2.1. Theoretical methods

The resonance electron attachment energies were calculated in the framework of the density-functional theory (DFT) and the time-dependent DFT (TDDFT) using a multi-basis-set TDDFT methodology (Thiam & Rabilloud 2021). The vertical electron affinity (VEA) was evaluated using DFT calculations (using the functional ωB97x (Chai & Head-Gordon 2008)) with the diffuse basis set aug-cc-pvtz (Kendall et al. 1992), while the anionic excitation energies were calculated using TDDFT and the cc-pvtz basis set. The latter, which did not include any diffuse function, was fully suitable to describe valence-type excitations while preventing the occurrence of intruder-discretized continuum states. Gibbs free energies of fragmentation were calculated at the ωB97x/aug-ccpvtz level at 90 K. All calculations were performed with the Gaussian16 suite of programs (Frisch et al. 2016). Pre- and postprocessing operations were performed using the graphical interface Gabedit (Allouche 2011). Calculations performed on H_2O can be found in a previous paper (Abdoul-Carime et al. 2022). Here, we only provide calculations on benzene.

2.2. Experimental methods

The experimental procedure is explained in detail elsewhere (Abdoul-Carime et al. 2022). Briefly, C_6H_6 (2.4 mbar) and H_2O (22.3 mbar) vapors were premixed at room temperature, forming an admixture of about 10% benzene and 90% water in a 27 mL mixing chamber prior to the injection into the measurement chamber at a base pressure of few 10^{-10} mbar; this was to be condensed onto an Au substrate held at 90 K by a closed-cycle He refrigerator. A volumetrically calibrated effusing gas quantity (MKS Baratron type 127) provided an estimate of the thickness of the deposited film. The typical thickness used here was approximately five MonoLayers (MLs) of molecules within ± 40% uncertainty. A pure water film of 1 ML corresponds to a thickness of 0.25 nm (Optiz et al. 2007). It is noteworthy that, in these experiments, knowledge of the exact thickness of the film was not necessary, but the film must be sufficiently thick to avoid possible effects of the metal substrate (i.e., quenching or enhancing process) and thin enough to minimize the multiple electron scattering (i.e., the mean free path of electrons in ice films is about 3 nm (Leclerc et al. 1987)) that would modify the energy of the reacting electrons. A monoenergetic electron beam (a few tenths of nA, ~ 0.3 cm^2), generated by a trochoidal electron monochromator to provide an energy selection of $\Delta E \sim 400$ meV, impinged normally to the substrate for 50 minutes. The electron energy was calibrated by a fast recording of the onset of the electron transmission curve (Sanche 1979). From the charging of the film during irradiation, this onset was rescaled every 30 s until no appreciable shift was observed. Otherwise, the film would be irradiated at different electron energies, and the fragmentation process—and perhaps the subsequent chemistry—would consequently be modified. After irradiation of the film by the electron beam at a given energy, the substrate was heated at a rate of 12 K/min for thermal desorption. The desorbed neutral species were detected by recording quadrupole mass spectrometry (QMS) in the "neutral" mode (Balzer). In the present experiments, the spectrometer was set at m/z 94 for the detection of phenol molecules. Note that we also observed the products formed by H_2O decomposition and reaction (namely H_2O_2), but they are not discussed here since they have already been considered in detail elsewhere (Pan et al. 2004). The yield of the neutral species was recorded as a function of the substrate temperature providing the so-called temperature-programmed desorption (TPD) spectrum. Each TPD spectrum was repeated from three to six times, providing the measurement fluctuations (c.a., ~ 40%), which can be associated with the accuracy of the presented data.

3. Results and discussion

Temperature-programmed desorption spectra of m/z 94 u (phenol) were recorded over a range of electron irradiation energies

[1] 10^5 electrons/MeV deposited: International Commission on Radiation Units and Measurements, Report 31. Average energy required to produce an ion pair, Bethesda, MD (1979).

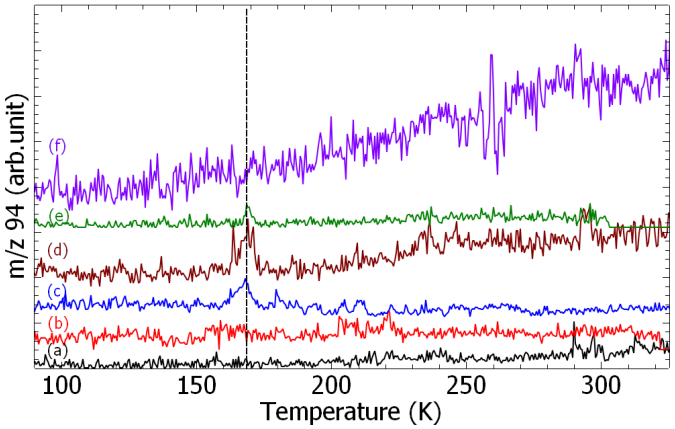

Fig. 1: Temperature-programmed desorption spectra of m/z 94 u (phenol) recorded after depositing a fresh film (*a* - black); 50 min electron irradiation at (*b* - red) 5 eV–50 nA, (*c* - blue) 7 eV–50 nA, (*d* - brown) 8 eV–133 nA, (*e* - green) 9 eV–91 nA and (*f* - purple) 13 eV–120 nA. The dashed line is a guides the eye.

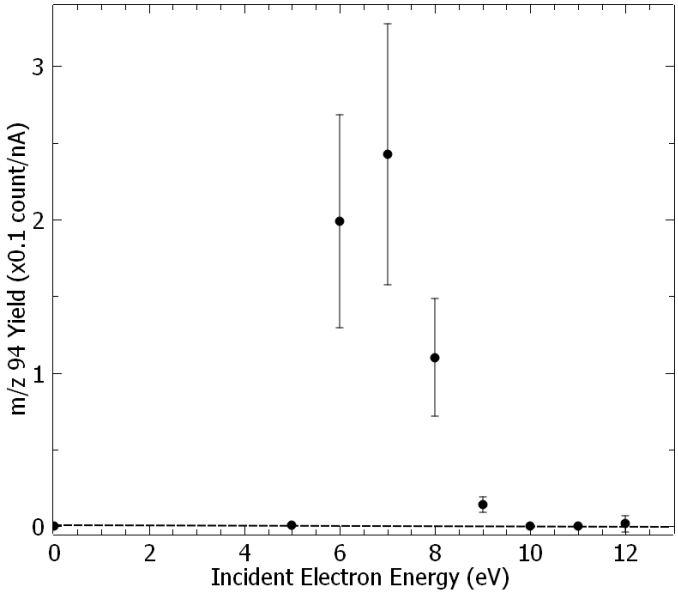

Fig. 2: Integrated phenol (C_6H_5OH) yield normalized to the electron current as the function of the electron energy. The error bars are estimated to be 40 % (see experimental method).

(0–13 eV) and electron currents (0–140 nA) as illustrated in Figure 1: (*a* - black) no irradiation, (*b* - red) 5 eV, (*c* - blue) 7 eV, (*d* - brown) 8 eV, (*e* - green) 9 eV, and (*f* - purple) 13 eV. Up to electron energies of 5 eV, this species is not observed, suggesting that it is not formed upon electron irradiation. From 6 to 10 eV, a feature is observed, peaking at 166 K, while disappearing for higher electron energies. TPD temperatures of pure phenol deposited onto Pt(111) and Ag(111) were measured to be 195 K (Ihm & White 2000) and 204 K (Lee et al. 2001), while that of H_2O from pure-water-ice adsorption on polycrystalline Au substrate was been reported to be 160 K (Collings et al. 2004). As the desorption temperature of phenol coincides with that of pure water, it seems that phenol molecules are mostly synthesized from benzene "embedded" in water ice rather at the gold surface. Thus, formed phenol molecules are expelled along with desorbed water molecules (Smith et al. 1997). The TPD peak is then integrated and normalized to the electron current (also convertible to electron dose for 50 min irradiation), for each irradiating energy. This yield, plotted as the function of the electron energy (Figure 2), presents a resonant feature at the electron energy of about 7 eV. This measured yield function is notably "sharply peaked" (6 eV–9 eV) in contrast to our previous work on electron irradiation of benzonitrile:water experiments performed at the same experimental conditions (Abdoul-Carime et al. 2024a). A broad structure in the 6–12 eV energy range, in addition to a sharp peak at 2 eV in the phenol yield function, was indeed reported.

Previous experiments on low-energy electron induced synthesis in two-reactant films (Abdoul-Carime et al. 2024a) have shown that at the energies below the typical ionization potential of most organic molecules (i.e., below 8–9 eV), the reactions are initiated by the fragmentation of specific molecules via dissociative electron attachment (DEA) (Illenberger & Momigny 1999). Briefly, the impinging free electron is initially captured by a molecule, forming a transient anion. The latter decays into dissociation for a negative anion fragment and at least one neutral counterpart. If the neutral fragment is a reactive radical, subsequent reactions may take place between the radical and the neighbouring molecules (Abdoul-Carime et al. 2024a; Abdoul-Carime & Kopyra 2025). The formation of the transitory negative ion arises either from (1) a shape (i.e., accommodation of the extra electron in a usually unoccupied molecular orbital (MO)) or (2) a core-excited resonance (i.e., the excitation of a valence electron in some excited state concomitantly to the capture of the extra electron by the molecular positive core). A third possibility is when DEA is mediated by the formation of a dipole-bound anion. This latter has been observed in the gas phase (Abdoul-Carime et al. 2024c), but it is unlikely formed in the condensed phase. Indeed, the dipole-bound character of the anion produced in isolation is lost in the presence of other interacting molecules (Desfrançois et al. 1995). DEA to H_2O has been well studied experimentally in the gas phase (Rawat et al. 2007), in molecular films (Pan et al. 2005), and theoretically (Abdoul-Carime et al. 2022; Faure et al. 2004; Lacombe et al. 2015). The dominant dissociation channel (by far) consists of the resonant production of the H^- anion in association with an $OH^\bullet$ radical at 7 eV and a threshold at round 6 eV (Rawat et al. 2007). Further fragmentation peaks have been reported at 9.2 eV and 12.6 eV (Rawat et al. 2007). The observed core-excited resonances implicate LUMO or LUMO+1 ← HOMO or HOMO-1 transitions concomitantly to the capture of the electron by the positive molecular core (Abdoul-Carime et al. 2022). For benzene, the gas-phase DEA experiments showed the resonant cleavage of the C-H bond for $C_6H_5^-$ anion and $^\bullet H$ radicals, as well as the fragmentation of the aromatic ring producing $C_2H_2^-$ anion at electron energies of around 8 eV and 9 eV (Fenzlaff & Illenberger 1984).

It was recently shown that the irradiation of benzene films by 10–1000 eV electrons produced H^- anions as the dominant anion fragment (Alvarez et al. 2024). In fact, for most hydrocarbon and aromatic molecules, electron-stimulated desorption from thin film experiments has shown that the production of the hydrogen anion is by far the dominant dissociation channel detectable (e.g., Rowntree et al. 1991; Ellis-Gibbings et al. 2017). The resonant features observed in DEA to benzene experiments (Fenzlaff & Illenberger 1984) are closely associated with the calculated resonances presented in Figure 3. Notably, the calculated resonances reflect the transition states, while the peak positions in experimental measurements are the convolu-

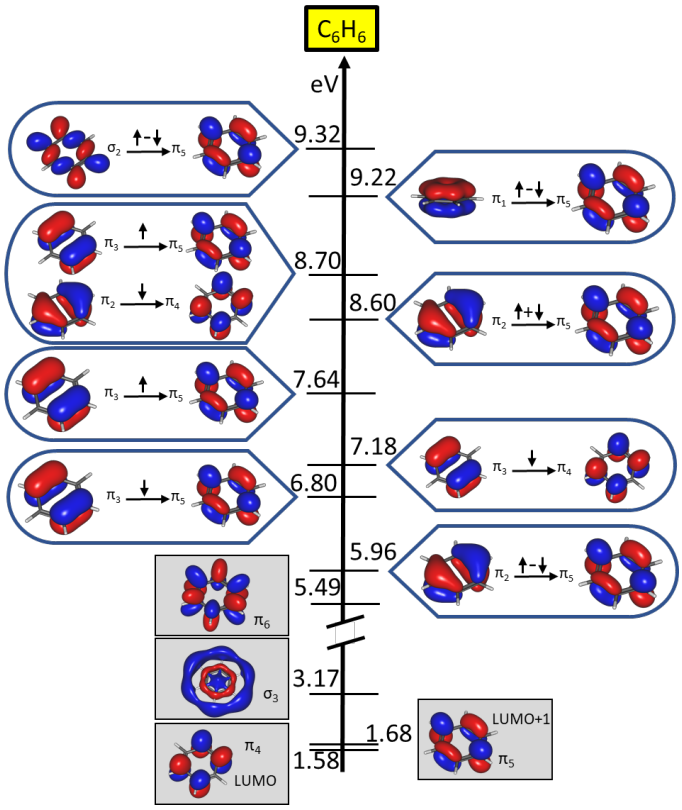

Fig. 3: Calculated attachment energies (in eV) relative to the neutral ground state of C_6H_6 are given together with the molecular orbitals involved in the trapping of the extra electron. The formation of this transitory anion arises from either the shape resonance (the orbital occupied by the extra electron is plotted on a gray background) or core-excited resonances when the trapping of the colliding electron into the LUMO occurs concomitantly with the promotion of a valence electron. The arrows indicate the spin of the implicated electron (↑ up, ↓ down), and "⟶" shows the transition.

tion of the attachment cross-sections (i.e., MOs) and the energy-dependent survival probability (Illenberger & Momigny 1999). The shape-resonance energies at 1.58, 1.68, and 5.5 eV (shaded in gray, Figure 1) agree with the R-matrix-calculated electron scattering cross-sections and the gas-phase experimental transmission experiments (Costa et al. 2019). Above 5.5 eV, our theory presents core-excited resonances consisting of the excitation of a core (valence) electron to some higher energy empty states. More interestingly, the MO transition is strongly electron-spin dependent (↑ and ↓ are electron-spin up and down states, respectively). Indeed, the $\pi_5 \leftarrow \pi_3$ transition energy depends on the spin electron transition: 6.8 eV and 7.64 eV for ↓ and ↑ electrons, respectively. The 8.60 eV, 9.22 eV, and higher resonances are associated with the linear combination of up and down spin electrons. It is to be noted that π states are non-dissociative unless this state crosses a dissociative σ^* state leading to the production of the negative fragments and their associated neutral counterparts; two asymptotic σ^* states were found to lead to $C_6H_5^-$ or H^- anion fragments, respectively (Figure 4). Gas-phase experiments on DEA with benzene have shown that the production of $C_2H_2^-$ possibly generated neutral C_4H_4 (Fenzlaff & Illenberger 1984); the latter species may be a bi-radical or, most likely, a stable, closed-shell molecule with m/z 52 with linear (e.g., HC≡C-C(H)=CH_2) or cyclic structures (Cremer et al. 2006). The present work has not clearly identified any species at m/z in the vicinity of 69 u or 86 u, associable with either C_4H_4OH or $C_4H_4OH_2$ compounds, respectively.

As the H^- anion is the most dominant fragment from the interaction of LEEs with both H_2O and C_6H_6, the concomitantly produced $OH^\bullet$ and $C_6H_5^\bullet$ radicals may interact either together, or with water or benzene molecules yielding phenol: C_6H_5OH (m/z 94). It is interesting to note here that the yield function shown in Figure 2 resembles to that of H^-/benzene (Fenzlaff & Illenberger 1984) (narrow energy resonance) and thus corroborates the key role played by the $OH^\bullet + C_6H_5^\bullet$ radical reaction.

Table 1: Calculated Gibbs free energy (eV) at 90 K for the formation of phenol.

Reaction	Gibbs Free Energy (eV)
$OH^\bullet + C_6H_5^\bullet \rightarrow C_6H_5OH$	-4.643
$OH^\bullet + C_6H_6 \rightarrow C_6H_5OH + H$	0.051
$C_6H_5^\bullet + H_2O \rightarrow C_6H_5OH + H$	0.256

Table 1 displays gas-phase-calculated energetics of possible secondary reactions by providing the Gibbs free energies. In the water-ice matrix, the exoergicity is expected to remain close to its gas-phase value, while barrier heights of transition states and intermediates might be slightly lowered or raised. Reaction (1), $OH^\bullet + C_6H_5^\bullet \rightarrow C_6H_5OH$, was calculated to be very exoergic by 4.6 eV. While reaction (2), $OH^\bullet + C_6H_6 \rightarrow C_6H_5OH$, is found endoergic by 51 meV, reaction (3), $C_6H_5^\bullet + H_2O \rightarrow C_6H_5OH$, is unlikely within the present experimental conditions, since it requires additional energy of ~260 meV to be activated. Reaction (1) may proceed via dissipation of the excess energy in the water-ice matrix or via the release of a UV photon not detectable by the present setup. While reaction (2) appears to be almost energetically accessible a priori, the process nevertheless requires a potential barrier of ~0.5 eV to be overcome (Hollman et al. 2011). Therefore, this reaction channel is not likely in the present experimental conditions.

The yield of production of phenol can be compared to that of the benzene in the c-C_6H_6/H_2O film deposited in the substrate. The number of ions, $N_{\rm ion}$, of $C_6H_6^+$ and $C_6H_5OH^+$ measured by the 70 eV electron ionization in the mass spectrometer can be estimated as $N_{\rm ion} \sim N_{\rm mol} N_e \sigma_{\rm mol} \epsilon$, where $N_{\rm mol}$ is the number of molecules, N_e the density of the ionizing electrons, $\sigma_{\rm mol}$ the ionization cross-section, and ϵ the collection efficiency. As 70 eV electron ionization cross-sections of benzene and phenol have been estimated to be 26.7 Å^2 (Singh et al. 2016) and 17.5 Å^2 (Gupta et al. 2019), respectively, from the present measurement of $N^+_{\rm phenol}/N^+_{\rm benzene}$ ~0.52% per μA electron current during a 50 min irradiation, we can estimate the production of phenol from benzene, $N_{\rm phenol}/N_{\rm benzene}$, to be about 2.6x10^{-4} per μC. The formation rate of phenol via the irradiation of the (10:90%) benzene:water film can be compared to a certain degree to that from the (4:96%) benzonitrile:water film (Abdoul-Carime et al. 2024a). For the latter, for 3 eV electron irradiation, this rate has been evaluated to be ~ 4.10^{-4}/μC per irradiated surface.

4. Conclusions

Past studies have shown that UV photolysis of PAHs in water ice leads to the replacement of peripheral H atoms by OH groups (Bernstein et al. 2002). In contrast, for the simplest aromatic hyr-

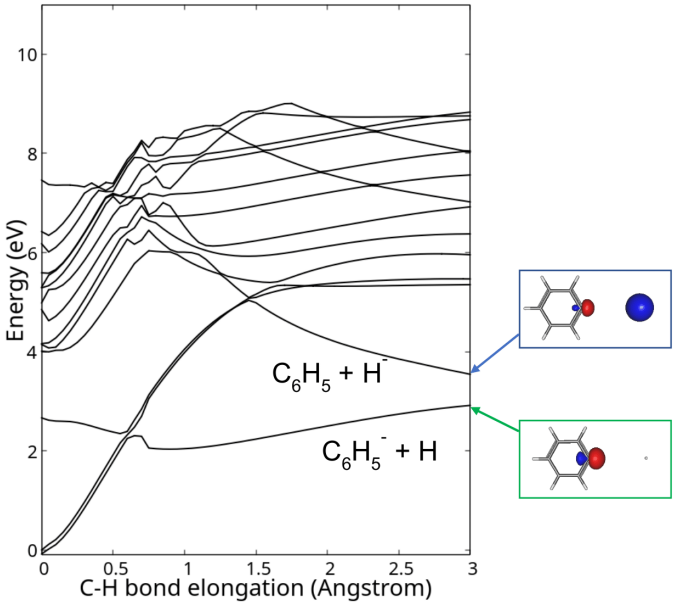

Fig. 4: Adiabatic potential energy curves (PEC) of the anion $C_6H_6^-$ calculated at the ωB97x/6-31G level. Two asymptotic σ^* states are found to lead $C_6H_5^-$ or H^- fragments, respectively. The orbital occupied by the extra electron is shown when the C-H bond elongation is equal to 3 Å.

docarbon, i.e., benzene, only O-heterocyclic benzene is clearly formed under UV irradiation of benzene–water ice, while phenol is tentatively detected (Materese et al. 2015). However, it has been shown that phenol can be generated in water–benzene systems via various pathways including catalytic conversion of benzoic acid (Fraga-Dubreuil et al. 2006), a radical–neutral C_6H_6 + $OH^\bullet$ reaction well above 300 K (Baulch et al. 2005), and the photolysis of a benzene and ozone mixture in argon matrices ($C_6H_6 + O_3 + h\nu$ (>280 nm) $\longrightarrow C_6H_6 + {}^\bullet O(^3P)$ (Parker & Davis 1999)).

We demonstrate that the irradiation of benzene molecules in a water-ice environment by low-energy (<12 eV) electrons also leads to the synthesis of phenol. The initial step consists of electron-induced dissociation of H_2O and C_6H_6, yielding $OH^\bullet$ and $C_6H_5^\bullet$ neutral radicals, respectively. Three subsequently different processes involving neutral radicals, respectively $OH^\bullet$ and $C_6H_5^\bullet$, are underlined: (1) $OH^\bullet$ + $C_6H_5^\bullet$, (2) $OH^\bullet$ + C_6H_6, and (3) $C_6H_5^\bullet$ + H_2O. In photolysis benzene/O_3 in argon matrix experiments (Parker & Davis 1999), the $O^\bullet$ radical may diffuse in the solid for a reaction. In the present work, we found that phenyl and hydroxyl radicals may also possibly diffuse before reacting since the deposited vapors, mainly containing water molecules, form amorphous ices (i.e., amorphous ice below 105 K and a crystalline structure above 120 K (Spisa et al. 2001). However, the structure of films may affect reactivity (Ghesquière et al. 2018; Garrod et al. 2022). Among the three mentioned processes, only (1) is energetically accessible. The present observations may be relevant in the context of reactions in meteorites (e.g., Tagish lake (Hilts et al. 2014), Murchinson, or Orgueil (Derenne & Robert 2010)) and, more broadly, to the chemistry of icy cores (Ghosh et al. 2022).

By showing that the functionalization of an aromatic species can be driven out by low-energy electrons, our study supports the view that Galactic cosmic rays characterized by energies above $\sim 10^{10}$ eV, triggering a cascade of low-energy electrons (≤20 eV) when impacting interstellar ices, can be a significant contributor (Wu et al. 2024) to the interstellar synthesis of prebiotic molecules whose delivery by comets, meteorites, and interplanetary dust particles may have kick-started life on Earth. Furthermore, it is desirable to incorporate low-energy electron-induced processes in current and future astrochemical simulation toolkits not only for water ices (Shingledecker et al. 2020), but more generally for cosmic ices (Wakelam et al. 2013). Such models are important for interpreting James Webb Space Telescope observations, which are currently being used to probe complex organic molecules found in ices near star-forming regions in the context of the interstellar heritage of the building blocks of life.

Acknowledgements. This study and the visit of E.O and S.C were supported by CNRS MITI – "Conditions Extrêmes 2024" (grant number 265810). In addition, F.R. thanks the GENCI-IDRIS for supporting the computing time through the grant A0150807662.

References

Abdoul-Carime, H. & Kopyra, J. 2025, Int. J. Mol. Sci., 26, 688
Abdoul-Carime, H., Lathuilière, B., Nedelec, P., & Kopyra, J. 2024a, Journal of Geophysical Research: Planets, 129, e2023JE008151
Abdoul-Carime, H., Thiam, G., & Rabilloud, F. 2024b, ChemPhysChem, 25, e202400287
Abdoul-Carime, H., Thiam, G., & Rabilloud, F. 2024c, J. Phys. Chem. Lett., 15, 10329
Abdoul-Carime, H., Thiam, G., Rabilloud, F., Charlieux, F., & Kopyra, J. 2022, ACS Earth Space Chem., 6, 1126
Allamandola, L. J., Tielens, A. G. G. M., & Barker, J. R. 1989, Astrophys J. Suppl., 71, 733
Allouche, A.-R. 2011, J. Comput. Chem., 32, 174
Alvarez, L., Bass, A. D., Lozano, A. I., et al. 2024, Physical Chemistry Chemical Physics, 26, 9197
Arumainayagam, C. R., Garrod, R. T., Boyer, M. C., et al. 2019, Chem Soc. Rev., 48, 2293
Baulch, D. L., Bowman, C. T., Cobos, C. J., et al. 2005, Journal of Physical and Chemical Reference Data, 34, 757
Bernard-Salas, J., Peeters, E., Sloan, G. C., et al. 2006, The Astrophysical Journal, 652, L29
Bernstein, M., Dworkin, J., Sandford, S., & Allamandola, L. 2002, Adv. Space Res., 30, 1501
Blanco, F., Munōz, A., Almeida, D., et al. 2013, Eur. Phys. J. D, 67, 199
Bohm, D. K. 1992, Chem. Rev., 92, 1487
Boyer, M. C., Rivas, N., Tran, A. A., Verish, C. A., & Arumainayagam, C. R. 2016, Surface Science, 652, 26
Bulak, M., Paaredkooper, D. M., Fedoseev, G., & Linnartz, H. 2013, A&A, 647, A82
Burkhardt, A. M., Lee, K. L. K., Changala, P. B., et al. 2021, ApJ Lett., 913, L18
Cabezas, C., Agúndez, M., Pérez, C., et al. 2025, A&A, 701, L8
Cernicharo, J., Agúndez, M., Cabezas, C., et al. 2021, A&A, 649, L15
Cernicharo, J., Heras, A. M., Tielens, A., et al. 2001, The Astrophysical Journal, 546, L123
Chai, J. & Head-Gordon, M. 2008, J. Chem. Phys., 128, 084106
Collings, M. P., Anderson, M. A., Chen, R., et al. 2004, MNRAS, 354, 1133
Costa, F., Alvarez, L., Lozano, A. I., et al. 2019, J. Chem. Phys., 151, 084310
Coustenis, A., Achterberg, R. K., Conrath, B. J., et al. 2007, Icarus, 189, 35
Cremer, D., Kraka, E., Joo, H., Stearns, J. A., & Zwier, T. S. 2006, Physical Chemistry Chemical Physics, 8, 5304
Derenne, S. & Robert, F. 2010, Meteoritic & Planetary Sci., 45, 1461
Desfrançois, C., Abdoul-Carime, H., Khelifa, N., & Schermann, J. P. 1995, Journal de Chimie-Physique, 92, 409
Ellis-Gibbings, L., Bass, A. D., Cloutier, P., García, G., & Sanche, L. 2017, Physical Chemistry Chemical Physics, 19, 13038
Faure, A., Gorefienkel, J., & Tennyson, J. 2004, J. Phys. B.: At. Mol. Opt. Phys., 37, 801
Fenzlaff, H. P. & Illenberger, E. 1984, Int. J. Mass Spectrom. Ion Proc., 59, 185
Fraga-Dubreuil, J., Serna, J., Garcia-Verdugo, E., et al. 2006, J. Supercritical Fluids, 39, 220
Frisch, M. J. et al. 2016, Gaussian 16, Revision C.01, Gaussian, Inc (Wallingford CT)
Garrod, R. T., Jin, M., Matis, K. A., et al. 2022, The Astrophys J. Supp. Series, 256, 1
Ghesquière, P., Ivlev, A., Noble, J. A., & Theulé, P. 2018, A&A, 614, A107

Ghosh, R., Sil, M., Kumar Mondal, S., et al. 2022, Research in Astronomy and Astrophysics, 22, 065021
Gupta, D., Choi, H., Singh, S., et al. 2019, J. Chem. Phys., 150, 064313
Hänni, N., Altwegg, K., Combi, M., et al. 2022, Nat Commun, 13, 3639
Hilts, R. W., Herd, C. D. K., Simkus, D. N., & Slater, G. F. 2014, Meteoritics & Planetary Science, 49, 526
Hollman, D., Simmonett, A., & Schaefer, H. 2011, PCCP, 13, 2214
Hrodmarsson, H. R., Aleman, I., Candian, A., et al. 2025, Space Science Reviews, 221, 42
Ihm, H. & White, J. M. 2000, J. Phys Chem. B, 104, 6202
Illenberger, E. & Momigny, J. 1999, in Gaseous molecular ions: an introduction to elementary processes induced by ionization, Edts H. Baümgartel E.U. Franck, W. Grünbein, Steinkopff (Berlin Heidelberg: Springer-Verlag,)
Kaiser, R. I. & Hansen, N. 2021, The Journal of Physical Chemistry A, 125, 3826
Kendall, R. A., Dunning Jr., T. H., & J., R. 1992, J. Chem. Phys., 96, 6796
Kodera, Y. & Hikida, T. 1990, J. Photochem. Photobiol A: Chemistry, 51, 437
Lacombe, L., Dinh, P. H. M., Rienhard, P.-G., Suraud, E., & Sanche, L. 2015, Eur. Phys. J. D, 69, 195
Lafosse, A., Bertin, M., Domaracka, A., et al. 2006, PCCP, 8, 5564
Langer, R., Maa, Q., & Pitsch, H. 2023, Combustion and Flame, 258, 112574
Leclerc, G., Goulet, T., Cloutier, P., Jay-Gerin, J.-P., & Sanche, L. 1987, J. Phys. Chem. A, 91, 4999
Lee, J., Ryu, S., & Kim, S. K. 2001, Surf. Sci., 481, 163
Leger, A. & Puget, J. L. 1984, Astronomy and Astrophysics, 137, L5
Lemmens, A. K., Rap, D. B., Brünken, S., Buma, W. J., & Rijs, A. M. 2022, PCCP, 24, 14816
Mason, N., Nair, B., Jheeta, S., & Szymanska, E. 2014, Faraday Discussions, 168, 235
Materese, C., Nuevo, M., & Sandford, S. 2015, The Astrophys. J., 800, 116
McMahon, S. J. & Prise, K. M. 2019, Cancers, 11, 205
Meinshein, W. G. 1963, Nature, 197, 833
Mucke, M., Braune, M., Barth, S., et al. 2010, Nature Physics, 6, 143
Öberg, K. I. 2016, Chem. Rev., 116, 9631
Optiz, A., Scherge, M., Ahmed, S. I.-U., & Schaefer, J. A. 2007, J. Appl. Phys., 101, 064310
Pan, X., Abdoul-Carime, H., Cloutier, P., Bass, A. D., & Sanche, L. 2005, Radiat. Phys. Chem., 72, 193
Pan, X., Bass, A. D., Jay-Gerin, J.-P., & Sanche, L. 2004, Icarus, 172, 521
Parker, J. K. & Davis, S. R. 1999, J. Am. Chem. Soc., 121, 4271
Pimblott, S. & LaVerne, J. 2007, Radiat. Phys. Chem., 76, 1244
Prasad, S. S. & Tarafdar, S. P. 1983, The Astrophys. J., 267, 603
Rawat, P., Prabhudesai, V. S., Aravind, G., & Rahman, M. A. 2007, J. Phys. B.: Atm. Mol. Opt. Phys., 40, 4625
Rowntree, P., Parenteau, L., & Sanche, L. 1991, The Journal of Physical Chemistry, 95, 4902
Ruiterkamp, R., Peeters, Z., Moore, M., Hudson, R., & Ehrenfreund, P. 1990, Astronomy and Astrophysics, 440, 391
Sabbah, H., Quitté, G., Demyk, K., & Joblin, C. 2024, Nat. Sci., 4, e20240010
Sanche, L. 1979, J. Phys. Chem., 71, 4860
Sandford, S. A., Aléon, J., Alexander, C. M. O., et al. 2006, Science, 314, 1720
Schuhmann, M., Altwegg, K., Berthelier, J.-J., et al. 2019, A&A, 630, A31
Sephton, M. A. 2005, Philosophical Transactions of the Royal Society A: Mathematical, Physical and Engineering Sciences, 363, 2729
Shingledecker, C., Incerti, S., Ivlev, A., et al. 2020, The Astrophys. J., 904, 189
Singh, S., Naghma, R., Kaur, J., & Antony, B. 2016, J. Chem. Phys., 145, 034309
Smith, R. S., Huang, C., Wong, E. K. L., & Kay, B. 1997, Phys. Rev. Lett., 79, 909
Snow, T. P. & Bierbaum, V. M. 2008, Annu. Rev. Anal. Chem., 1, 229
Spisa, S. L., Waldheim, M., Lintemoot, J., et al. 2001, J. Geophys. Res., 106, 351
Thiam, G. & Rabilloud, F. 2021, J. Phys. Chem. Lett., 12, 9995
Tribett, P., Yarnall, Y., Gerakines, P. A., Hudson, R., & Materese, C. 2026, The Astrophys. J., 997, 291
Wakelam, V., Cuppen, H. M., & Herbst, E. 2013, in Astrochemistry and astrobiology, ed. ts (C. S. Cockell, S. Leach, chapt 4, Springer: I. W. M. Smith)
Wenzel, G., Cooke, I. N., Changala, P. B., et al. 2024
Wu, Q. T., Anderson, H., Watkins, A. K., et al. 2024, ACS Earth and Space Chemistry, 8, 79
Yoon, Y. H., Hörst, S. M., Hicks, R. K., et al. 2014, Icarus, 233, 233